International Journal of Biological Macromolecules 69 (2014) 369–381

Contents lists available at ScienceDirect

International Journal of Biological Macromolecules

journal homepage: www.elsevier.com/locate/ijbiomac

Multivariate analysis for resolving interactions of carbidopa with dsDNA at a fullerene-C_{60}/GCE

Mohammad-Bagher Gholivand[a,*], Ali R. Jalalvand[a,b], Hector C. Goicoechea[b]

[a] Faculty of Chemistry, Razi University, Kermanshah 671496734, Iran
[b] Laboratorio de Desarrollo Analítico y Quimiometría (LADAQ), Cátedra de Química Analítica I, Universidad Nacional del Litoral, Ciudad Universitaria, CC 242 (S3000ZAA) Santa Fe, Argentina

ARTICLE INFO

Article history:
Received 17 February 2014
Received in revised form 19 May 2014
Accepted 20 May 2014

Keywords:
Carbidopa
dsDNA
Fullerene-C_{60}
Voltammetry
Spectroscopy
Chemometrics
Molecular docking

ABSTRACT

For the first time, interactions of carbidopa (CD) with double-stranded calf thymus DNA (dsDNA) in a phosphate buffered solution (PBS, 0.05 M, pH = 4.0) at a fullerene-C_{60}/glassy carbon electrode (FLR/GCE) has been studied by cyclic voltammetry (CV), linear sweep voltammetry (LSV), and square wave voltammetry (SWV). The interaction of CD with dsDNA was also monitored using fluorescence (F) and UV–vis spectroscopic techniques. New information was obtained when a row- and column-wise augmented matrix consisting of SWV, LSV, F and UV–vis data was resolved using multivariate curve resolution-alternating least squares (MCR-ALS) as a powerful chemometric tool. Pure electrochemical and spectroscopic signals of CD, dsDNA and dsDNA–CD_2 complex, and their concentration profiles were then successfully resolved. Molecular docking studies confirmed that the binding of CD with dsDNA shows minor groove binding mode which was in accordance with experimental results. Under optimized conditions, the SWV responses were linearly related to dsDNA concentration between 0.1 and 25.0 nM and a limit of detection (LOD) of 0.03 nM was calculated ($3S_b/b = 3$). Moreover, the modified electrode exhibited long term stability, good repeatability, and reproducibility, and high sensitivity and selectivity toward dsDNA determination in human serum samples, demonstrating its feasibility toward dsDNA sensing.

1. Introduction

Carbidopa (CD, Fig. S1, Supplementary Information) is a drug given to people with Parkinson's disease in order to inhibit peripheral metabolism of levodopa. This property is significant in that it allows a greater proportion of peripheral levodopa to cross the blood brain barrier for central nervous system effect. The CD inhibits aromatic-L-amino-acid decarboxylase (DOPA decarboxylase or DDC) [1] an enzyme important in the biosynthesis of L-tryptophan to serotonin and in the biosynthesis of levodopa to dopamine.

The dsDNA contains all of the genetic information as well as it plays a very important role in life processes. Thus, in order to obtain the biochemical mechanisms of prevention and treatment of human diseases, great efforts have been made to investigate the interaction between dsDNA and drug molecules [2,3]. Moreover, nucleic acids interaction with drugs is a fundamental issue in life phenomena. This process is associated with molecular recognition in dsDNA hybridization, gene mutations, sensing of bioactive agents such as anticancer drugs, and action mechanism of some dsDNA-targeted drugs [4–6].

Fullerenes (FLR) have been widely studied attributing to their unique structural, electronic and spectroscopic properties since their discovery by Kroto et al. in 1985 [7,8]. They have also been exploited for diverse applications in the fields of biology, chemistry and nanoscience [9,10]. As every carbon in a FLR (C_{60}) is a surface atom, the electron transport of this material is highly sensitive to the surface-adsorbed molecules [11]. Especially, as an electron acceptor, C_{60} displays rich electrochemistry because of its unique dimensional and electronic structures [12].

There are many methods to study the dsDNA binding properties, including surface plasmon resonance [13], luminescence [14], capillary electrophoresis [15], NMR [16], circular dichroism [17], UV–vis spectrophotometry [18], fluorescence [19] and

Abbreviations: CD, carbidopa; dsDNA, double-stranded calf thymus DNA; FLR, fullerene-C60; GCE, glassy carbon electrode; CV, cyclic voltammetry; LSV, linear sweep voltammetry; SWV, square wave voltammetry; DPV, differential pulse voltammogram; F, fluorescence; MCR-ALS, multivariate curve resolution-alternating least squares; LOD, limit of detection; PBS, phosphate buffered solution; SEM, scanning electron microscope; EFA, evolving factor analysis; PCA, principal component analysis; SVD, singular value decomposition; lof, lack of fit; RSD, relative standard deviation.

* Corresponding author. Tel.: +98 831 4274557; fax: +98 831 4274559.
E-mail addresses: mbgholivand2013@gmail.com, mbgholivand@yahoo.com (M.-B. Gholivand).

http://dx.doi.org/10.1016/j.ijbiomac.2014.05.074
0141-8130/

electrochemistry [20–22]. Among these, electrochemical and spectroscopic techniques offer the advantages of high sensitivity and selectivity. However, for complex systems of more than two components, it is usually difficult to distinguish these existing species because their response signals often overlap. This limitation can be overcome with the use of multivariate analysis [23].

Multivariate curve resolution-alternating least squares (MCR-ALS) is a soft-modeling method, which is based on factor analysis, and can be used to analyze spectroscopic data from biomolecular systems at equilibrium in solution [24]. MCR-ALS allows mathematical analysis of more than one data matrix simultaneously, which greatly reduces the number of solutions inherent in the factor analysis model. Extension of the common multivariate spectral studies with the use of the MCR-ALS method has also been carried out on the interaction equilibrium of dyes and drugs with biomolecules [25–27]. The MCR-ALS method may be applied to all original voltammetric and spectroscopic measurements, obtained by one or several techniques; its output provides the concentration profiles and pure signals of all the chemically analyzed components: the concentration profiles provide the information on the mechanism of the dsDNA process, and the features of the recovered pure signals help to identify the species involved.

The main objectives of the present study were:

1. Literature survey revealed that no attempt has been made to study the interaction of CD with dsDNA till date therefore, this motivated us to employ a combination of experimental and computational approaches to determine where and how CD binds to dsDNA.
2. To perform simultaneous analysis for the reactants mentioned above and their complex product as a function of concentration, and to carry out this analysis with the aid of different techniques, CV, LSV, SWV, F, UV–vis, and molecular docking so as to obtain different information about the above interaction as well as the thermodynamic parameters involved.
3. To construct a combined data matrix from the voltammetric and spectroscopic measurements by means of the augmented matrix approach, and then, to analyze this information with the use of the MCR-ALS chemometric method so as to resolve the overlapping reactant/product profiles.
4. Exploiting a quantitative concept from the studied interaction for selective and sensitive determination of dsDNA in human serum samples.

2. Experimental and theoretical details

2.1. Experimental details

2.1.1. Chemicals and solutions

Double-stranded calf thymus DNA (dsDNA) was purchased from Sigma (St Louis, MO, USA). Carbidopa was purchased from SERVA (Feinbiochemica Heidelberg/New York). FLR (C_{60}, 99.9%) was purchased from Sigma (St Louis, MO, USA). All other chemicals of analytical grade were purchased from Merck (Darmstadt, Germany) and used without further purifications. Purified water from a Milli-Q-RO4 water purification system (Millipore, Bedford, MA, USA, provided by Kermanshah Oil Refining Company) with a resistivity higher than 18.0 MΩ cm was used to prepare all solutions. Phosphate buffered solution (PBS, 0.05 M, pH 4.0) was prepared using NaH_2PO_4, and Na_2HPO_4. $[Fe(CN)_6]^{3-/4-}$ solution (redox probe, 5.0 mM) was prepared in PBS (0.05 M, pH 4.0) and used for some of experiments. The stock solutions of dsDNA (0.01 M) and CD (0.01 M) were prepared in PBS (0.05 M, pH 4.0) and stored at 4 °C in a refrigerator until use. Dilutions were done just prior to use. The concentration of dsDNA was calculated according to the absorbance at 260.0 nm by using $\varepsilon_{DNA} = 6600.0\ mol^{-1}\ L\ cm^{-1}$ [28].

2.1.2. Instruments and software

All fluorescence spectra were measured on a Cary Eclipse fluorescence spectrophotometer equipped with a 1.0 cm quartz cuvette. The UV–vis spectra were measured on an Agilent 8453 UV–vis Diode-Array spectrophotometer controlled by the Agilent UV–vis ChemStation software. Electrochemical experiments were performed using a μ-Autolab TYPE III, Eco Chemie BV, Netherlands, and driven by the NOVA software (Version 1.8). A conventional three-electrode cell was used with a saturated calomel electrode (SCE) as reference electrode, a Pt wire as counter electrode and a modified glassy carbon electrode (GCE) as working electrode. KYKY-EM 3200 scanning electron microscope (SEM) was used for surface image measurements. Viscosity measurements were made using a viscometer (SCHOT AVS 450) which termostated at 25 ± 0.5 °C by a constant temperature bath. A JENWAY-3345 pH-meter equipped with a combined glass electrode was applied for the pH measurements. The three-dimensional structure of FLR was generated using Nanotube Modeler software. The chemical structure of the CD was constructed by Hyperchem package (Version 8.0) and energy minimization for CD was performed by AM1 semi empirical method with Polak-Ribiere algorithm until the root mean square gradient of 0.01 kcal mol^{-1}. The crystal structure of the dsDNA (PDB ID: 1BNA) was downloaded from the Protein Data Bank [29]. The Molegro Virtual Docker (MVD) software was employed to generate a docked conformation of CD with dsDNA. The MCR-ALS was implemented using the graphical interface provided by Prof. Tauler in his web page [30]. The recorded experimental data was smoothed, when necessary, and converted to matrices by means of several homemade MATLAB (Version 7.14) programs. EQUISPEC program was run in MATLAB environment. A simple homemade MATLAB program was used for computing the concentrations of CD and dsDNA and their ratio in all voltammetric and spectroscopic experiments. All computations were performed on a DELL XPS laptop (L502X) with Intel Core i7-2630QM 2.0 GHz, 8 GB of RAM and Windows 7-64 as its operating system.

2.1.3. Fabrication of FLR/GCE and dsDNA/FLR/GCE

Prior to the electrode modification, the GCE surface was polished with PK-4 polishing kit, BASi MF-2060 successively followed by rinsing thoroughly with redistilled deionized water until a mirror like finish was obtained. It was then dipped in a beaker containing 0.2 M H_3PO_4 solutions to remove the adhered powder, rinsed with distilled water and dried at room temperature for 10.0–15.0 min. Stock solution of FLR was prepared by dissolving its solid powder in CH_2Cl_2 (0.50 mg mL^{-1}). A known volume (40.0 μL) of this solution was adsorbed onto the surface of the clean and dried GCE using a micropipette and dried under room temperature. The FLR film formed was then reduced in 1.0 M KOH in the potential range 0.0 to −1.5 V at 10.0 mV s^{-1}. The resulting electrode is called FLR/GCE. A known volume (20.0 μL) of 4.0 mg mL^{-1} dsDNA solution was adsorbed onto the surface of FLR/GCE and allowed to be dried in air for 45.0 min at room temperature. The resulting electrode is called dsDNA/FLR/GCE. Then modified electrodes were kept at 4.0 °C in a refrigerator until use.

2.1.4. Procedures

Solutions used in the fluorescence and UV–vis experiments were prepared in PBS (0.05 M, pH 4.0) containing appropriate amounts of dsDNA and CD. The total added volume (dsDNA or CD) was less than 0.2 mL. Titrations were performed manually using suitable micropipettes. A mixed solution was shaken thoroughly and equilibrated for 5.0 min. Fluorescence or UV–vis spectra were then recorded.

Solutions used in the voltammetric experiments were prepared in PBS (0.05 M, pH 4.0) containing appropriate amounts of dsDNA and CD. The total added volume (dsDNA or CD) was less than 0.4 mL. A given CD–dsDNA system was stirred for 10.0 s, and then the sample was analyzed as required.

2.1.5. Development of the augmented matrix for MCR-ALS

Experiment 1 ($\mathbf{D}^{CD}_{SWV}$): The concentration of CD was kept constant (3.0×10^{-4} M), and dsDNA was added to the solution in the range of 0.0–3.0×10^{-4} M.
Experiment 2 ($\mathbf{D}^{dsDNA}_{SWV}$): The concentration of dsDNA was kept constant (1.0×10^{-4} M), and CD was added to the solution in the range of 0.0–5.0×10^{-4} M.
Experiment 3 ($\mathbf{D}^{CD}_{LSV}$): The concentration of CD was kept constant (5.0×10^{-4} M), and dsDNA was added to the solution in the range of 0.0–5.0×10^{-4} M.
Experiment 4 ($\boldsymbol{D}^{dsDNA}_{LSV}$): The concentration of dsDNA was kept constant (2.0×10^{-4} M), and CD was added to the solution in the range of 0.0–1.0×10^{-3} M.
Experiment 5 ($\mathbf{D}^{CD}_{F}$): The concentration of CD was kept constant (3.0×10^{-7} M), and dsDNA was added to the solution in the range of 0.0–3.0×10^{-7} M.
Experiment 6 ($\mathbf{D}^{dsDNA}_{F}$): The concentration of dsDNA was kept constant (1.0×10^{-7} M), and CD was added to the solution in the range of 0.0–5.0×10^{-7} M.
Experiment 7 ($\mathbf{D}^{CD}_{UV-vis}$): The concentration of CD was kept constant (5.0×10^{-6} M), and dsDNA was added to the solution in the range of 0.0–5.0×10^{-6} M.
Experiment 8 ($\mathbf{D}^{dsDNA}_{UV-vis}$): The concentration of dsDNA was kept constant (1.0×10^{-6} M), and CD was added to the solution in the range of 0.0–5.0×10^{-6} M.

2.2. Theoretical details

The MCR-ALS method for the analysis of electroanalytical data is summarized elsewhere [31,32], and here only a working summary is provided. The goal of MCR is to decompose composite measured profiles such as voltammograms or spectra into the different pure profiles for each species in a mixture. The resulting extracted information for the pure components may be in the form of single bands or more complex profiles. Such data can be arranged into $\boldsymbol{D}$ (M × N) matrix with M objects and N variables, e.g. wavelength or potential. The MCR decomposition of a matrix is carried out according to the following equation:

$$\mathbf{D} = \mathbf{C}\mathbf{S}^{T}\mathbf{+E} \quad (1)$$

where $\boldsymbol{D}$ is the matrix of the experimental data, with dimensions of M × N. The matrix, $\boldsymbol{C}$ (M × P), describes the concentration profiles of the P species involved in the given measured profiles. The matrix, $\boldsymbol{S}^{T}$ (P × N), is then the contribution of the measured profiles of these P species in the N columns of the data matrix (pure signals' profiles). $\boldsymbol{E}$ (M × N) is the matrix of residuals, which contains the data variance unexplained by the product, $\boldsymbol{CS}^{T}$. One important and frequently used iterative approach to solve Eq. (1) is MCR by alternating least squares (ALS). The optimization process starts from initial guesses of $\boldsymbol{C}$ and $\boldsymbol{S}^{T}$, and these are then refined to yield profiles with chemical meaning.

When the same chemical system is monitored using more than one technique, e.g. SWV, LSV, F and UV–vis, a matrix is constructed, which consists of row- and column-wise augmented data, i.e. four types of information are presented. The individual data matrices corresponding to the four types of technique are placed side-by-side. The related model for MCR-ALS analysis is shown below:

$$\begin{bmatrix} \boldsymbol{D}^{CD}_{SWV}\boldsymbol{D}^{CD}_{LSV}\boldsymbol{D}^{CD}_{F}\boldsymbol{D}^{CD}_{UV-vis} \\ \boldsymbol{D}^{dsDNA}_{SWV}\boldsymbol{D}^{dsDNA}_{LSV}\boldsymbol{D}^{dsDNA}_{F}\boldsymbol{D}^{dsDNA}_{UV-vis} \end{bmatrix} = \begin{bmatrix} \boldsymbol{C}^{CD} \\ \boldsymbol{C}^{dsDNA} \end{bmatrix} [\boldsymbol{S}^{T}_{SWV}\boldsymbol{S}^{T}_{LSV}\boldsymbol{S}^{T}_{F}\boldsymbol{S}^{T}_{UV-vis}] + [\boldsymbol{E}_{SWV}\boldsymbol{E}_{LSV}\boldsymbol{E}_{F}\boldsymbol{E}_{UV-vis}] \quad (2)$$

If $\boldsymbol{D}_{SWV}$ $\boldsymbol{D}_{LSV}$ $\boldsymbol{D}_{F}$, and $\boldsymbol{D}_{UV-vis}$ are the data obtained with the four techniques, there are two matrices of concentration profiles, $\boldsymbol{C}^{CD}$ and $\boldsymbol{C}^{dsDNA}$, and four row-wise augmented matrices of measured profiles, $\boldsymbol{S}^{T}{}_{SWV}$, $\boldsymbol{S}^{T}{}_{LSV}$, $\boldsymbol{S}^{T}{}_{F}$, and $\boldsymbol{S}^{T}{}_{UV-vis}$, which contain the pure signals for the techniques used to obtain $\boldsymbol{D}_{SWV}$ $\boldsymbol{D}_{LSV}$ $\boldsymbol{D}_{F}$, and $\boldsymbol{D}_{UV-vis}$, respectively.

When the augmented matrix of the four data matrices is being built, the number of analyte species, F, can be obtained with the aid of evolving factor analysis (EFA) [33] or principal component analysis (PCA) or other methods based on factor analysis. The EFA method provides an estimation of the regions or windows where the concentration of different components is changing or evolving, and it also provides an initial estimation of how these concentration profiles change during the experiment. This method is based on the evaluation of the magnitude of the eigenvalues associated with all the submatrices of a matrix built up by adding successively all the rows of the original data matrix. The calculation is performed in two directions: forward (in the direction of the experiment) and backward (in the opposite direction of the experiment), e.g. Abdollahi and Mahdavi illustrate how concentration profiles obtained from EFA may be used as initial estimates for the concentration matrix input in the constrained ALS optimization [34]. PCA, an alternative approach to EFA, is a common chemometrics tool; it yields the number and direction of the relevant sources of variation in a bilinear data set [35]. Once the PCs, P, are determined and an initial estimate of their concentration profiles is obtained, it becomes easier to obtain improved estimates of either the concentration values or pure signals' profiles. Constraints in ALS optimization are implemented to facilitate the finding of pure or most representative contributions to the data matrix using real variables. The resolution methods start with initial estimates of $\boldsymbol{C}$ and work by optimizing iteratively the concentration, while introducing the available information about the system [35]. During the optimization, the suitable constraints are applied to ensure that the final solution is chemically meaningful [36]. The lack of fit (lof) [37], which is defined as the difference between the input data, $\boldsymbol{D}$, and the data reproduced from the $\boldsymbol{CS}^{T}$ product obtained by MCR-ALS, was used as a parameter to evaluate the goodness of fit of the model according to the following expression:

$$\mathrm{lof}(\%) = 100\sqrt{\frac{\sum_{i,j} e^{2}_{i,j}}{\sum_{i,j} d^{2}_{i,j}}} \quad (3)$$

where d_{ij} is an element in the raw data and e_{ij} is the corresponding residual after the model variation is removed.

However, the solutions to Eq. (1) obtained by MCR-ALS are not unique. They can have rotational and intensity ambiguities. To solve this limitation, column- and row-wise augmentation schemes (Eq. (2)) can be used for simultaneous resolution. This kind of simultaneous data analysis is more powerful compared to that described by Eq. (1) and allows for improved resolution of very complex data structures. In general, this method should be useful to overcome some uncertainties in the analysis of the data related to coincidental processes or small signal shifts. Thus, in this work, an augmented data matrix, was constructed and resolved by the MCR-ALS approach.

However, because of the combination of completely different types of data, e.g. voltammetric and spectroscopic data some

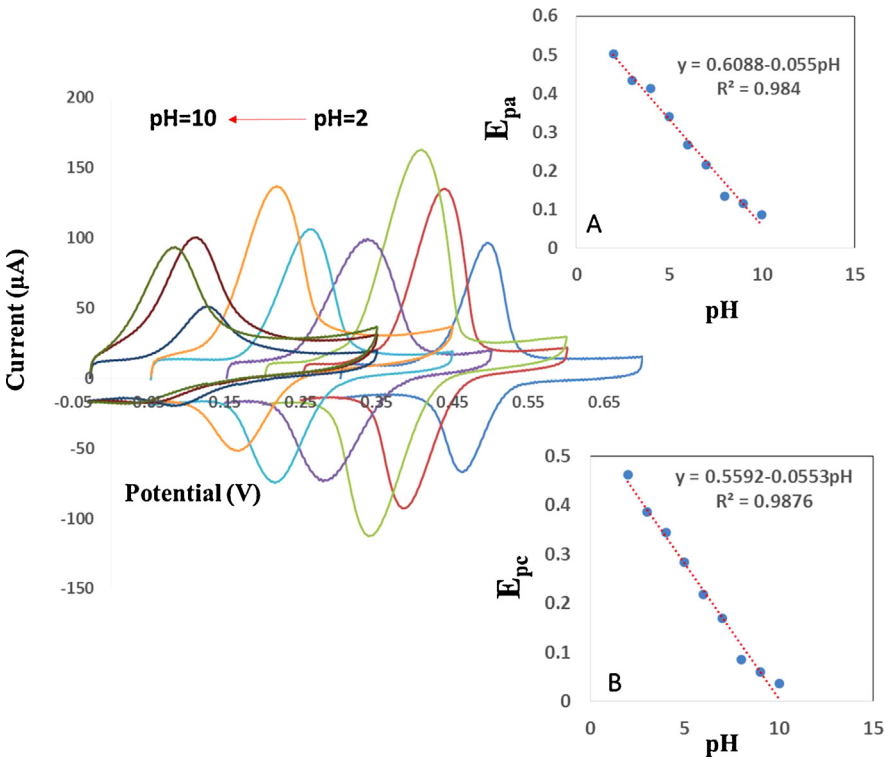

Fig. 1. Influence of solution pH on the voltammograms of 0.1 mM CD in PBS (0.05 M) at FLR/GCE, scan rate is 50.0 mV s^{-1}. Insets A and B are the variations of E_{pa} and E_{pc} vs. pH, respectively.

considerations must be performed in the analysis of the augmented matrix:

1. Due to the fact that voltammetric and spectroscopic signals are of very different magnitude, submatrices must be scaled in order to have a similar weight on the iterative ALS optimization of the augmented data matrix; in a first approach, this is done by dividing submatrices by their maximum values prior to their combination into an augmented data matrix.
2. The concept of component is a critical point. For spectroscopic data component is associated to pure chemical species in solution [38,39], but for electrochemical data component must be associated to a single electrochemical process giving a signal, including not only redox processes but also some other possible phenomena like, for instance, electrode adsorption of a species [31,32] or capacitive currents due to the charging of the electrical double layer at the electrode surface. Anyway, in many situations, a single electrochemical process is produced by a single species.
3. Taking into account the impossibility of applying a closure constrain (i.e. the mass balance) to the matrices obtained at different concentration levels, a normalization of the signals has been made along the MCR-ALS iterations. Considering that such normalization should be common to SWV, LSV, F, and UV–vis parts of each pure signal, it has been made by dividing the pure signal by its maximum absolute value (alternative normalization procedures have been tested but the results were similar).
4. To combine voltammetric and spectroscopic sub-matrices into an augmented matrix, all sub-matrices must contain the same number of rows and columns and must share the same distribution of the chemical species along the experiments. Ideally, this condition can be fulfilled using exactly the same total concentrations of CD and dsDNA in all titrations, but this is not possible because the concentrations required for voltammetric experiments are higher than those for spectroscopic ones. Thus, in the present work, voltammetric and spectroscopic experiments have been performed at different total concentrations but at the same values of ratio.

3. Results and discussion

3.1. Effects pH

In general, pH is one of the variables, which commonly affects the current and shape of voltammograms. Thus, it is important to investigate the effects of pH on electrochemical systems. Cyclic voltammograms of 0.1 mM CD solution at different pHs of the PBS (0.05 M) and at the scan rate of 50.0 mV s^{-1} were recorded (Fig. 1). As can be seen, when the pH changes from 2.0 to 10.0, both the anodic and the cathodic peak potentials shift to less positive potentials, and obey the following equations: $E_{pa}(V) = 0.6088–0.055pH$ and $E_{pc}(V) = 0.5592–0.0553pH$ (see the insets A and B of Fig. 1). The slopes of plots are close to the theoretical value of 0.0585 V/pH for a reversible redox reaction, so the number of electrons and protons involved in the reaction mechanism is equal. According to these results, in order to obtain a high sensitivity for quantitative purposes a pH value of 4.0 was selected for further experiments.

3.2. Effects of ionic strength

The interaction of CD with dsDNA at the FLR/GCE was also investigated under various NaCl concentrations (Fig. S2) to study the effects of ionic strength on interaction of CD with dsDNA and also to verify the mechanism of binding of CD to dsDNA. At low ionic strengths, the peak current response of 1.0 mM CD in PBSs (0.05 M, pH 4.0) in the presence of 0.5 mM dsDNA decreases with increasing NaCl concentration, while at high ionic strengths, a leveling-off was observed. In the intercalative mode, since the drug insert into the base pair pockets of dsDNA, the ionic strength does not affect the current response [40,41]. Therefore, variation of current versus

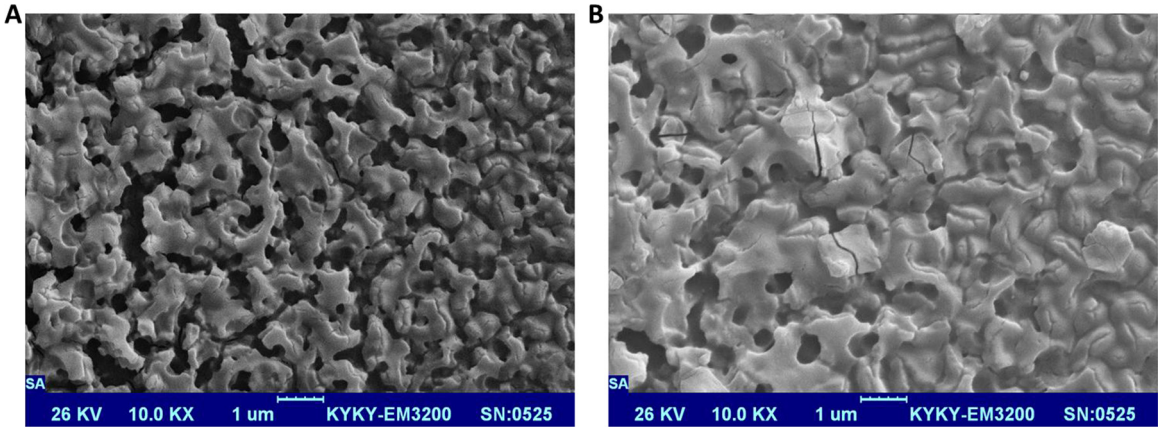

Fig. 2. SEM images of (A) FLR/GCE, and (B) dsDNA/FLR/GCE.

ionic strength indicated that CD could not be bound to the dsDNA by intercalation. But exact judgment about the mechanism of binding of CD to dsDNA will be postponed until seeing the results of next studies.

3.3. Effect of scan rate

The CVs of CD in PBS (0.05 M, pH 4.0) at various scan rates (υ) were recorded (not shown) on the surface of both FLR/GCE (free CD) and dsDNA/FLR/GCE (bound CD–dsDNA). Both anodic (I_{pa}) and cathodic (I_{pc}) peak currents were found to be linearly dependent on $\upsilon^{1/2}$ in the range of 50.0–350.0 mV s^{-1} at FLR/GCE which indicated that the redox process was controlled by diffusion. While the obtained results confirmed a totally irreversible oxidation for CD at the dsDNA/FLR/GCE and variation of I_{pa} vs. υ in the range of 50.0–350.0 mV s^{-1} was found to be linearly dependent on υ which confirmed that the oxidation process was controlled by adsorption at the dsDNA/FLR/GCE.

3.4. Surface morphology of FLR/GCE and dsDNA/FLR/GCE

Fig. 2A and B shows the SEM images of FLR/GCE and dsDNA/FLR/GCE. The SEM image of FLR/GCE clearly shows deposition of FLRs at the surface of the GCE (Fig. 2A). When dsDNA was immobilized on the electrode surface the dim FLR image became bright and the surface morphology changed with packing the FLRs (Fig. 2B).

3.5. Cyclic voltammetric studies of dsDNA–CD interaction

Useful information about the interaction of drugs and biological macromolecules usually can be acquired from the cyclic voltammetry that is one of the most important electroanalytical techniques due to the similarity among various redox chemical and biological processes. Therefore, cyclic voltammetry was used to study the electrochemical behavior of CD with dsDNA at the FLR/GCE. Fig. 3A compares the cyclic voltammograms of CD (0.1 mM) in PBS (0.05 M, pH 4.0) at bare GCE (curve a) and FLR/GCE (curve b). As can be seen, FLR/GCE exhibited excellent electrocatalytic behavior for oxidation of CD in comparison with the bare GCE. The CD shows a reversible oxidation at the FLR/GCE (Fig. 3B, curve a), which may be related to the oxidation of —OH groups (Scheme 1). When dsDNA was added to the CD solution (Fig. 3B, curves b–i) both oxidation and reduction peaks decreased markedly and shifted to less and more positive potentials, respectively, which indicate that CD interacts with dsDNA.

There are some possibilities for the decrease of the peak currents; they include an increase in viscosity of the solution or a blockage of the electrode surface by dsDNA adsorption; Wang et al. [42] carried out further CV experiments to clarify the observations. Their work involved the use of $[Fe(CN)_6]^{3-/4-}$ solution in the absence and presence of dsDNA. Therefore, cyclic voltammograms of 5.0 mM $[Fe(CN)_6]^{3-/4-}$, which cannot interact with dsDNA were recorded in PBS (0.05 M, pH 4.0) at FLR/GCE in the absence (Fig. 3C, curve a) and presence of dsDNA (Fig. 3C, curve b). As it can be seen in the presence of dsDNA, cyclic voltammograms of $[Fe(CN)_6]^{3-/4-}$ did not change significantly, so it can be concluded that the decrease of peak currents of CD after addition of dsDNA was caused by binding of CD to dsDNA and formation of the bulky dsDNA–CD_m complex (m is the stoichiometric coefficient) which slowly diffuses. This step was carried out to show that the decrease in peak currents is the result of complex formation and not due to blockage of the electrode surface by an adsorbed layer of dsDNA.

3.6. Determination of binding constant (K_b) and Hill coefficient (m) of dsDNA–CD_m complex

According to the method of Qu et al. [43], it is assumed that dsDNA and CD only produced a single complex dsDNA–CD_m according to the following reaction scheme:

$$\text{dsDNA} + m\,\text{CD} \leftrightarrow \text{dsDNA–CD}_m \quad (4)$$

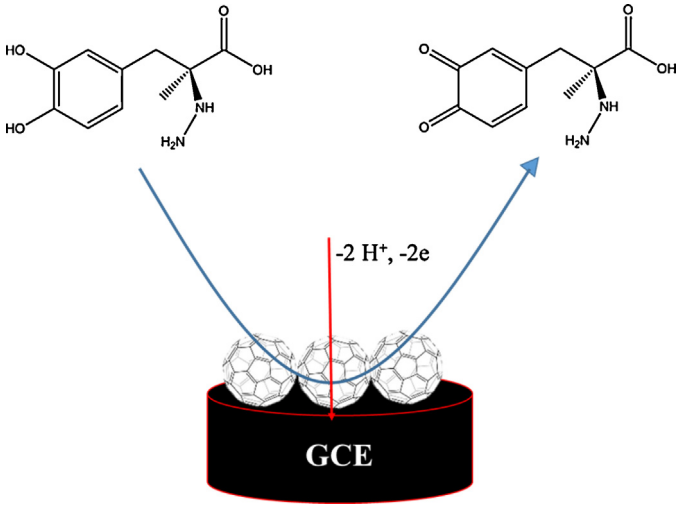

Scheme 1. Schematic representation of the methodology employed to FLR/GCE.

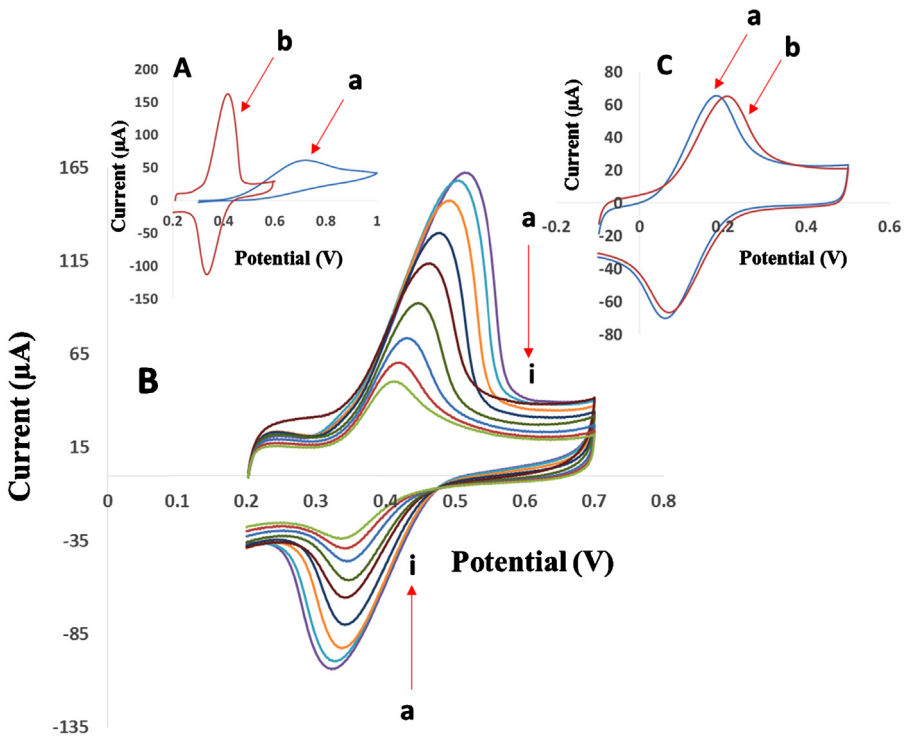

Fig. 3. (A) Cyclic voltammograms of 0.10 mM CD in PBS (0.05 M, pH 4.0) at (a) bare GCE, and (b) FLR/GCE; (B) cyclic voltammograms of 0.10 mM CD in PBS (0.05 M, pH 4.0) at FLR/GCE with different concentrations of dsDNA (a–i): 0.0–0.10 mM (in steps of 1.25×10^{-5} mM); and (C) cyclic voltammograms of 5.0 mM $[Fe(CN)_6]^{3-/4-}$ in PBS (0.05 M, pH 4.0): (a) in the absence of dsDNA and (b) in the presence of 5.0 mM dsDNA. In all cases scan rate was 50.0 mV s^{-1}.

The height of peak current (I) of the differential pulse voltammogram (DPV) is most sensitive to the equilibrium constant of dsDNA–CD_m complex. The decreasing value of I is proportional to the concentration of dsDNA–CD_m complex. In terms of the all-or-none (Hill) cooperative of multiple ligand binding [44,45], the fraction of dsDNA to which CD is bound as dsDNA–CD_m, relative to the total dsDNA concentration in the supporting electrolyte $[dsDNA]_0 = [dsDNA–CD_m]_{max}$ is given by:

$$f = \frac{[dsDNA–CD_m]}{[dsDNA–CD_m]_{max}} = \frac{[CD]^m}{([CD]^m + k_d^m)} \quad (5)$$

$$k_d^m = [CD]^m(1-f)/f \quad (6)$$

where $[dsDNA–CD_m]_{max}$ is the maximum concentration of complexed binding sites, [CD] is the concentration of free CD, K_d is the dissociation equilibrium constant and m is the Hill coefficient. Note that $K_d = [CD]_{0.5}$, i.e. at half occupation. The binding constant K_b is given by the reciprocity: $K_b = K_d^{-1}$. It is not advisable to use the overall constant $K = (K_b)^m$, which would have the physically meaningless dimension of M^{-m}. The interaction partners for CD are the binding sites of dsDNA. Mass conservation dictates that:

$$[dsDNA] = [dsDNA–CD_m]_{max} - [dsDNA–CD_m] \quad (7)$$

$$[CD] = [CD]_0 - m[dsDNA–CD_m] \quad (8)$$

where $[CD]_0$ is the total concentration of CD.

According to the following equation [46]:

$$I = k[CD] \quad (9)$$

where k is a constant. In line with this relationship the current difference ΔI is defined as:

$$\Delta I = k([CD]_0 - [CD]) = k \cdot m[dsDNA–CD_m] \quad (10)$$

$$\Delta I_{max} = k \cdot m[dsDNA–CD_m]_{max} \quad (11)$$

$$\log\left[\frac{f}{(1-f)}\right] = m \log\left(\frac{K_b}{M^{-1}}\right) + m \log\left[\frac{CD}{M}\right] \quad (12)$$

$$\log\left[\frac{\Delta I}{\Delta I_{max} - \Delta I}\right] = m \log K_b + m \log[CD] \quad (13)$$

Fig. 4 shows the plot of $\log[\Delta I/(\Delta I_{max} - \Delta I)]$ vs. $\log[CD]$ from the recording DPVs of CD at varying concentration (0.00–0.25 mM) and constant concentration of dsDNA (0.05 mM) in PBS (0.05 M, pH 4.0) at FLR/GCE. The Hill coefficient m can be obtained from the slope of Eq. (13) as 2.08 which proves that the binding ratio of dsDNA–CD_m complex is 1:2. Moreover, the value of K_b was calculated to be 3.11×10^4 M^{-1}.

3.7. Linear sweep and square wave voltammetric studies

Typical LSVs of dsDNA (1.0×10^{-4} M) in the presence of increasing concentrations of CD in the range of 0.0–5.0×10^{-4} M are shown in Fig. 5A. As can be seen, the peak current increased with the increase in concentration of the CD. There was also a possible positive peak shift developing as well. With these observations, there was little strong evidence to suggest the formation of dsDNA–CD_m complex, and consequently, it appeared that the increase in peak current was due mostly to the presence of free CD. Another possible explanation could be that the nature of the structural changes induced in dsDNA during its interaction with CD. The oxidation peak of the free CD and those of dsDNA overlap, and the recorded profile was the sum of these two phenomena, which increased together with the addition of CD.

Typical SWVs of dsDNA (2.0×10^{-4} M) in the presence of increasing concentrations of CD in the range of 0.0–1.0×10^{-3} M are shown in Fig. 5B. The observed variations are the same as LSV

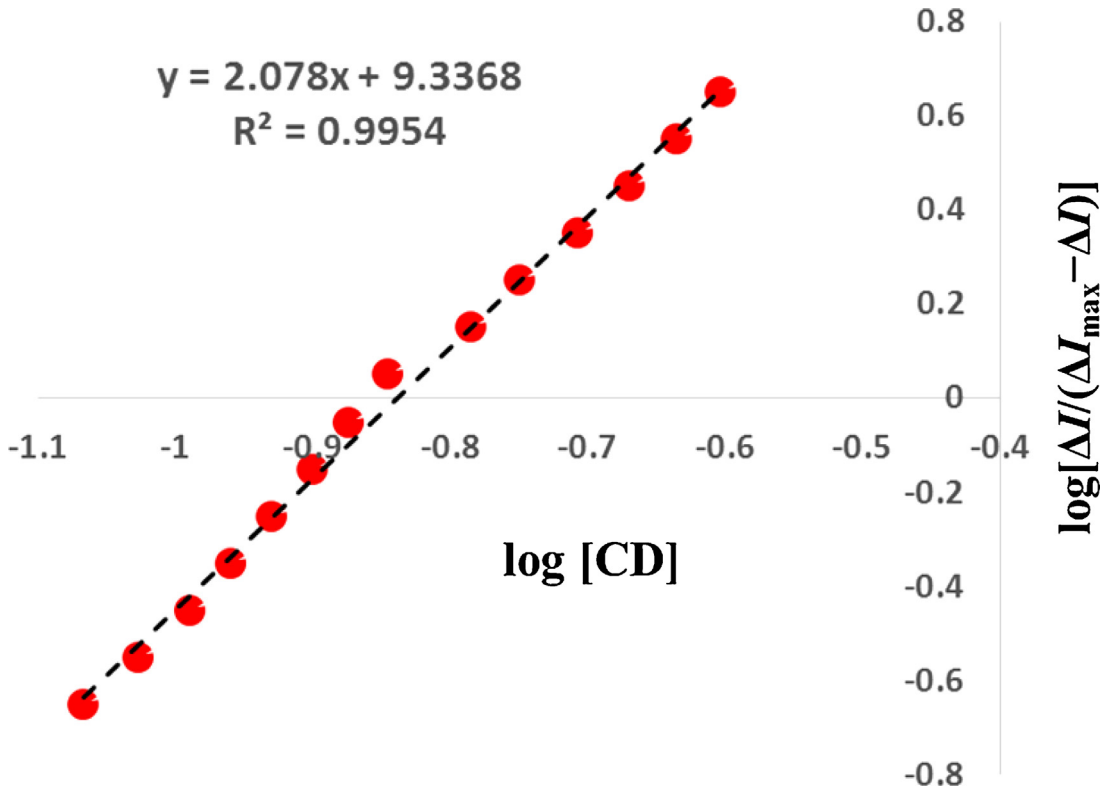

Fig. 4. The plot of $\log[\Delta I/(\Delta I_{max} - \Delta I)]$ vs. log [CD] from the recorded DPVs of CD at varying concentrations (0.0–0.25 mM) and constant concentrations of dsDNA (0.05 mM) in PBS (0.05 M, pH 4.0) at FLR/GCE.

measurements which need the same justifications. Therefore, we think repeating them is redundant.

3.8. Viscosity measurements

Viscometery is an effective tool to determine the mechanism of action of a drug at the dsDNA. A classical intercalation binding requires the space of adjacent base pairs to be large enough to accommodate the bound small molecules and to elongate the double helix, resulting in an increase of dsDNA viscosity (η) [47]. In contrast, there is little effect on the viscosity of dsDNA if groove binding occurs in the binding process [48]. The dsDNA viscosity experiments performed at 25 °C. Increasing amounts of the CD (r_i = 0–1) were used to evaluate viscosity η of the dsDNA. The values of relative specific viscosity $(\eta/\eta_0)^{1/3}$ versus $1/R$ (R = [dsDNA]/[complex]) were plotted (Fig. S3). Little change on the viscosity of dsDNA showed that the CD bound to dsDNA by groove binding [48,49].

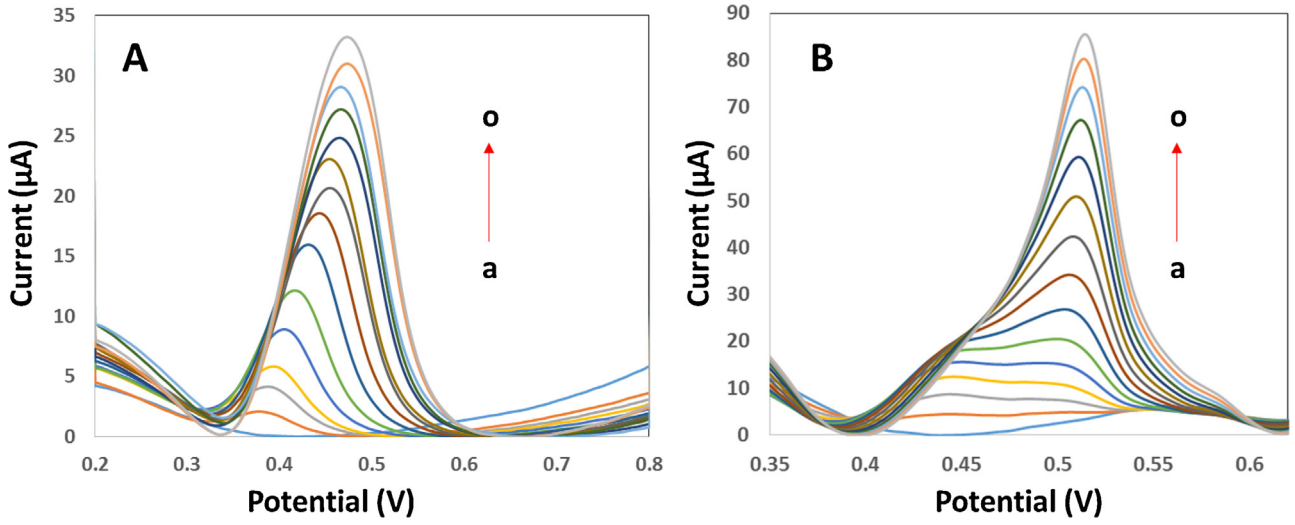

Fig. 5. (A) The LSVs of 1.0×10^{-4} M dsDNA in PBS (0.05 M, pH 4.0) in the presence of increasing concentrations of CD in the range of 0.0–5.0×10^{-4} M, and (B) Typical SWVs of 2.0×10^{-4} M dsDNA in PBS (0.05 M, pH 4.0) in the presence of increasing concentrations of CD in the range of 0.0–1.0×10^{-3} M.

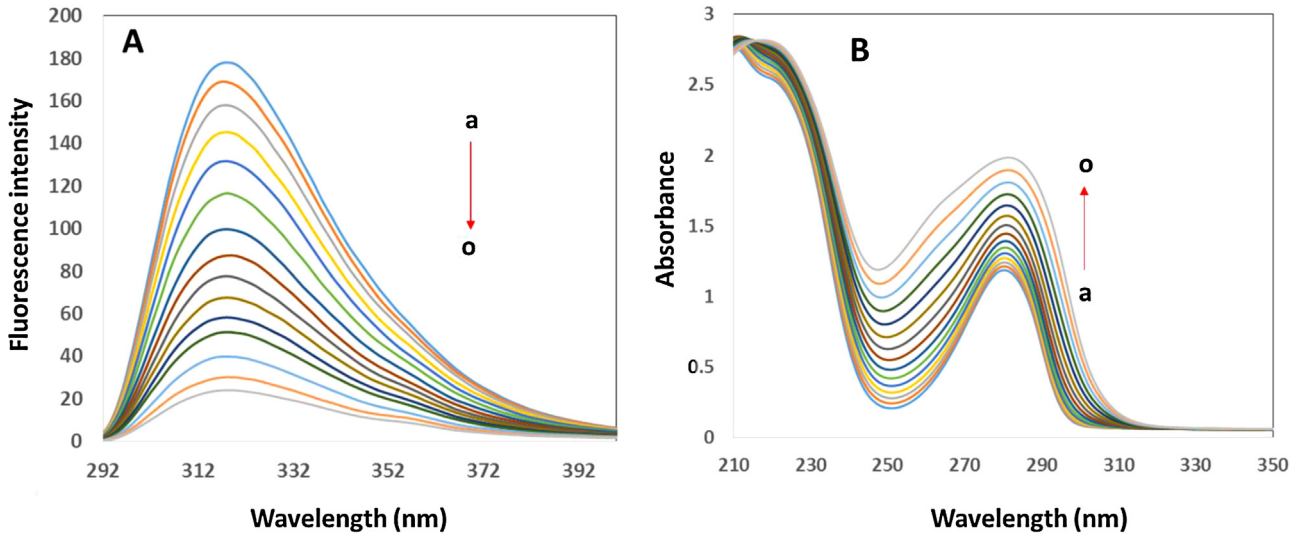

Fig. 6. (A) Fluorescence emission spectra of 3.0×10^{-7} M CD in the presence of increasing concentrations of dsDNA in the range of 0.0–3.0×10^{-7} M, λ_{ex} = 270.0 nm, and (B) UV–vis absorption spectra of 5.0×10^{-6} M CD in the presence of increasing concentrations of dsDNA in the range of 0.0–5.0×10^{-6} M.

3.9. Fluorescence quenching studies

The interaction of CD with dsDNA was also investigated by fluorescence spectroscopy. Solution of free CD displays intrinsic fluorescence with maximum excitation and emission wavelengths at 270 and 318 nm, respectively, whereas dsDNA has no fluorescence. Fig. 6A shows the fluorescence spectra of CD (3.0×10^{-7} M) in PBS (0.05 M, pH 4.0) in the absence (curve a) and presence of different dsDNA concentrations in the range of 0.0–3.0×10^{-7} M (curves b–o). It can be seen that addition of different concentrations of dsDNA to a fixed concentration of CD caused a decrease in the CD fluorescence intensity, indicating the quenching of CD fluorescence intensity upon binding to dsDNA.

Fluorescence quenching refers to any process, which decreases the fluorescence intensity of a sample, and quenching mechanisms are usually classified as dynamic or static. They are distinguished by their different temperatures and viscosity dependence; thus, dynamic quenching depends on diffusion, and therefore, the biomolecular quenching constants are expected to increase with increasing temperature. In contrast, increased temperature is likely to result in lower values of the static quenching constants.

For fluorescence quenching, the decrease in intensity is usually described by the well-known Stern–Volmer equation [50]:

$$\frac{F_0}{F} = 1 + K_{SV}[Q] \tag{14}$$

where F_0 and F denote the steady-state fluorescence intensities in the absence and in the presence of the quencher. K_{SV} is the Stern–Volmer quenching constant, and [Q] is the concentration of the quencher (dsDNA). The degree of fluorescence quenching as a function of temperature when dsDNA was added to CD, was clearly discernable but moderate. The values of K_{SV} (Table 1) decreased with increase in temperature, which indicated that the probable quenching mechanism of this interaction was initiated by the formation of a complex rather than by dynamic collision.

Table 1
Stern–Volmer quenching constants at different temperatures for the interaction of CD with dsDNA.

T (K)	K_{SV} ($\times 10^5$ M^{-1})	R^2
298.15	6.35	0.9978
304.15	5.81	0.9981
310.15	5.12	0.9821

The binding constant K_b and the binding sites m, when small molecules bind independently to a set of equivalent sites on a macromolecule, can be calculated using the following equation [51]:

$$\log\left[\frac{(F_0 - F)}{F}\right] = \log K_b + m \ \log[\text{dsDNA}] \tag{15}$$

K_b and m was obtained from double-logarithm linear curve (not shown) of $\log[(F_0 - F)/F]$ vs. $\log$ [dsDNA] as 3.98×10^4 M^{-1} and 2.12, respectively.

3.10. UV–vis absorption studies

Electronic UV–vis absorption spectroscopy is often employed to ascertain the bonding of foreign molecules with dsDNA. As previously mentioned there are two binding models for binding of small molecules to dsDNA: (1) groove binding and (2) intercalative binding, in which the small molecule or the drug intercalates into the relatively nonpolar interior part of the dsDNA helix. In general, changes in position of the band (red shift) and in absorbance (hypochromism) indicate that the small molecule has intercalated between dsDNA base pairs which is a strong interaction between the aromatic chromophore and the base pairs. The spectral effects have been rationalized as follows: the empty π^*-orbital of the small molecule couples with the π-orbital of the dsDNA base pairs, which causes an energy decrease, and a decrease of the $\pi \rightarrow \pi^*$ transition energy. Therefore, the absorption of the small molecule should exhibit a red shift. At the same time, the empty π^*-orbital is partially filled by electrons, reducing the transition probability, and this leads to hypochromism [52].

To investigate the interaction of CD with dsDNA, the absorption spectra of CD with various concentrations of dsDNA were recorded to obtain more information about the interaction mode (Fig. 6B). In PBS (0.05 M, pH 4.0), CD exhibits an absorbance peaks at 277.0 nm and it was found that with increasing of dsDNA concentration, the absorbance was increased obviously (hyperchromism). No red shift was observed in the spectra, which represents that the binding mode is not the intercalative binding [53] and these

hyperchromism changes indicated that the binding mode of CD to dsDNA might be groove binding [54,55].

Further discussion of the CD–dsDNA interaction on the basis of direct observations of the measured profiles was difficult, and multivariate analysis previously discussed was applied to extract further information, especially as function of concentration of the CD and dsDNA reactants.

3.11. Interpretation of the MCR-ALS results

For building an augmented matrix for the simultaneous resolution by MCR-ALS all voltammetric and spectroscopic data were collected from the two different types of experiment (a constant concentration of CD in the presence of increasing concentrations of dsDNA or a constant concentration of dsDNA the presence of increasing concentrations of CD, see Section 2.1.5 for more details). Fig. 7A and B shows LSVs and SWVs of CD (5×10^{-4} M) in the presence of increasing concentrations of dsDNA in the range of 0.0–5.0×10^{-4} M. Fig. 7C shows the fluorescence spectra of dsDNA (1.0×10^{-7} M) in the presence of increasing concentrations of CD in the range of 0.0–5.0×10^{-7} M, and Fig. 7C shows the fluorescence spectra of dsDNA (1.0×10^{-7} M) in the presence of increasing concentrations of CD in the range of 0.0–5.0×10^{-7} M. As previously discussed in detail (Section 2.2), the eight individual data matrices obtained from SWV, LSV, F, and UV–vis in Figs. 5–7 were combined into an augmented data matrix (first term of Eq. (2)), and then this augmented matrix was submitted for simultaneous resolution by the MCR-ALS (Eq. (2)) as a powerful chemometric tool. The intention was to extract information regarding: (i) any dsDNA–CD_m complex, and (ii) the relative concentrations of the various reactant and product species. Before starting the resolution, the number of contributions to the augmented matrix was determined by SVD and here, the SVD detected three components. These three components may be related to free CD, free dsDNA and one dsDNA–CD_m complex spices. Taking into account that MCR-ALS needs information as real as possible to start the resolution, the $\boldsymbol{C}$ matrix was estimated by the use of the EFA. EFA was basically designed to work with full rank two-way data sets and straightforward analysis of rank-deficient matrix does not provide useful information. To overcome this limitation, de Juan et al. [56] have recently proposed an evolution of the original algorithm. This new approach is based on a two-step strategy. First, rotational ambiguity is eliminated by matrix augmentation. The augmented data matrix is formed by column- and row-wise augmented data set. Then, EFA is applied to the unfolded full rank augmented data set eventually providing information about contributions that are otherwise hidden. PCA was also employed to select the appropriate number of components to describe the four systems, and it was found that the first three PCs explained 99.9% of the total data variance in the combined matrix [57]. Thus, both the EFA and PCA methods estimate the same number of factors or chemical species involved. Also, the required initial estimates of the concentration profiles for these three postulated species were obtained from the EFA results, and were used to start ALS optimization. Below, the used constraints in the iterative ALS optimization are described:

Non-negativity: this constraint is the most used in resolution methods and prevents the presence of negative values in profiles. It was applied to both concentration and signal profiles because their values are always positive.
Unimodality: this constraint was applied to signal profiles.
Closure: applying a closure constraint to the matrices obtained at different concentration levels is impossible.

By applying the mentioned constraints, the ALS optimization was started. As previously mentioned, the lof which is defined as the difference between the input data ($\boldsymbol{D}$) and the data reproduced from the product ($\boldsymbol{CS}^{T}$) obtained by MCR-ALS, was used as a parameter to evaluate the goodness of fit of the model. In this work, the best lof value was found to be 7.24% which implies that almost all of the variability in the experimental data presented as a product of the extracted signals and the concentration profiles, is explained. Standard deviation of the residuals was also found to be 0.018.

The results of MCR-ALS are shown in Fig. 8A–F. Fig. 8A showed that the concentration of dsDNA is decreasing and a new complex species is forming upon the addition of CD. As can be seen, the concentration of the complex spices increased sharply and reached to a maximum at the ratio, $r_{dsDNA/CD} \sim 5$. Therefore, it may be concluded that the complex species is a 1:2 dsDNA–CD complex species. On the other hand, Fig. 8B showed that with the mole-ratio method, the concentration of the dsDNA–CD complex increased and reached equilibrium when the ratio, $r_{CD/dsDNA} \sim 2.0$ which confirmed that that the complex species is a 1:2 dsDNA–CD complex species.

The pure voltammetric and spectral profiles extracted by the application of the MCR-ALS (Fig. 8C–F) provided new qualitative information about the nature of the complex. From these figures the valuable information about the nature of the involved complex species in each technique could be obtained. According to these results, it is clear that the complex species is electroactive at the FLR/GCE. The extracted fluorescence spectrum (Fig. 8E) of the dsDNA–CD_2 complex was obtained for the first time, and was the first such spectral representation of the dsDNA–CD_2 complex. Not surprisingly, its peak maximum fell between the CD and dsDNA bands at $\lambda = 318$ nm. The extraction of the voltammetric and spectroscopic profiles and their reasonable agreement with the measured data indicated that the MCR-ALS was applied successfully.

By comparing the results obtained by MCR-ALS with those of experimental techniques, it can be found that voltammetric and spectroscopic methods were successful to obtain the number and also the stoichiometries of the involved complex species.

3.12. Hard-modeling approach

In the case of hard-modeling approaches, a model is applied to guide the decomposition of matrix $\boldsymbol{D}$ following Eq. (1). As an example, in the case of dsDNA-drug interaction, the model includes the stoichiometry of the species formed, as well as initial trial value for the binding constant. This value is used to build an initial estimation of the concentration profiles included in $\boldsymbol{C}$. Once this estimation is obtained, a least squares fit is performed to obtain the pure spectra in $\boldsymbol{S}^{T}$ that best match the concentration profiles in $\boldsymbol{C}$ and the data in $\boldsymbol{D}$. A residual matrix $\boldsymbol{E}$ is then calculated from the difference between the data in $\boldsymbol{D}$ and the reproduced data matrix. The optimization procedure continues by tuning the stoichiometry of the proposed species until a desired level of residuals $\boldsymbol{E}$ is reached. A more detailed explanation of the mathematical basis of the algorithms used in these calculations can be found in Dyson et al. [58].

EQUISPEC, a hard-modeling algorithm, was applied to an augmented matrix (combined spectroscopic and voltammetric data) to compute the binding constants and also verify the results of Sections 3.6 and 3.9. The results of this study are shown in Table 2. As can be seen, there is a good agreement between the binding constant values computed by EQUISPEC and also with the results reported at Sections 3.6 and 3.9.

3.13. Molecular modeling studies

In the recent years, docking studies has provided insight into the interactions between macromolecules and ligands, which can substantiate the experimental results. In this study, the

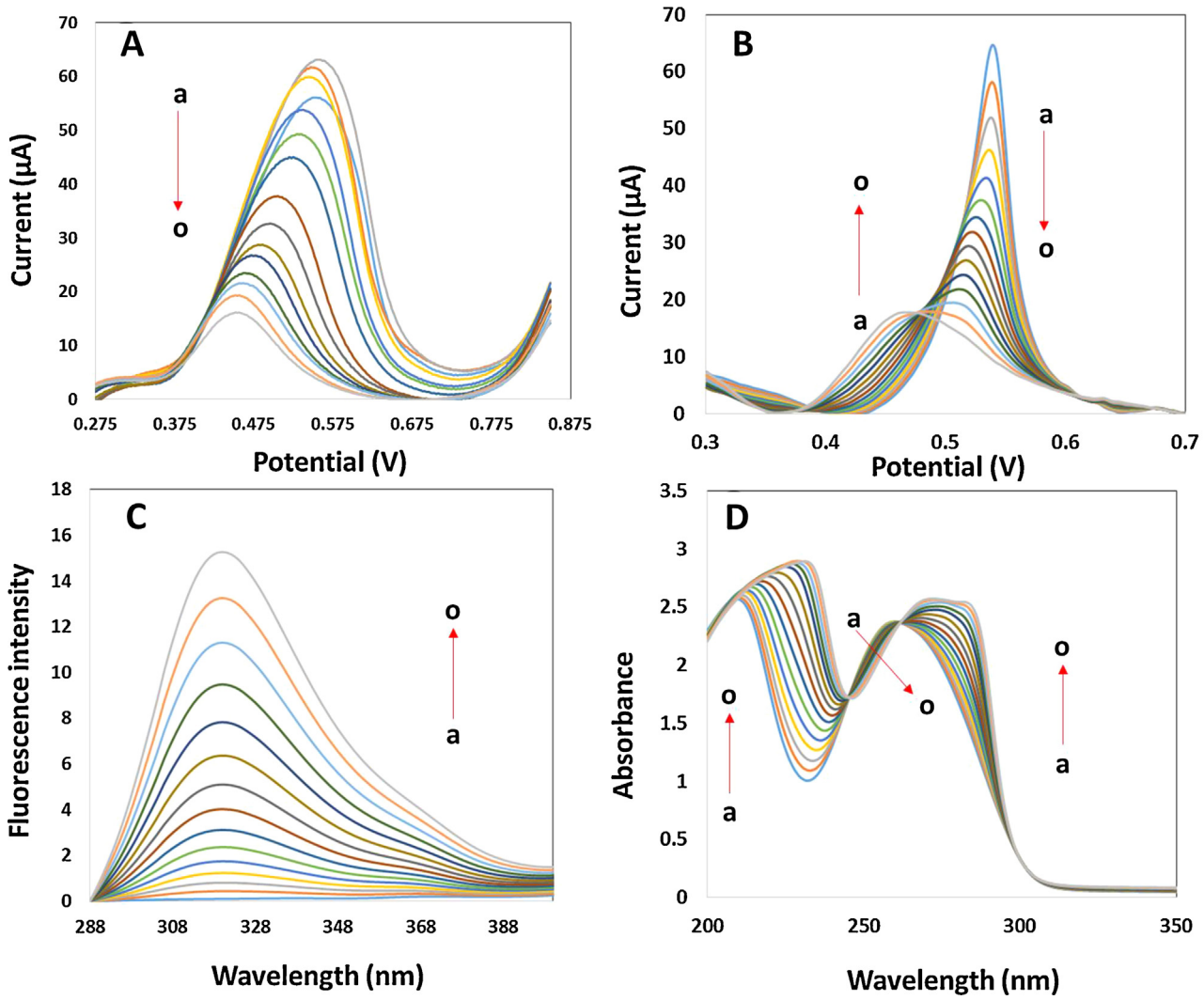

Fig. 7. (A) The LSVs of 5.0×10^{-4} M CD in PBS (0.05 M, pH 4.0) in the presence of increasing concentrations of dsDNA in the range of 0.0–5.0×10^{-4} M; (B) the SWVs of 5.0×10^{-4} M CD in PBS (0.05 M, pH 4.0) in the presence of increasing concentrations of dsDNA in the range of 0.0–5.0×10^{-4} M; (C) fluorescence emission spectra of 1.0×10^{-7} M dsDNA in PBS (0.05 M, pH 4.0) in the presence of increasing concentrations of CD in the range of 0.0–5.0×10^{-7} M, λ_{ex} = 280.0 nm; and (D) UV–vis absorption spectra of 1.0×10^{-6} M dsDNA in PBS (0.05 M, pH 4.0) in the presence of increasing concentrations of CD in the range of 0.0–5.0×10^{-6} M.

Molegro Virtual Docker (MVD) software was used to characterize the binding mode of CD at the dsDNA. Fig. 9A shows the groove binding of CD to the minor groove of dsDNA. It is well known that the interactions of chemical species with the minor groove of dsDNA differ from those occurring in the major groove, both in terms of electrostatic potential and steric effects, because of the narrow shape of the former. Small molecules interact with the minor groove, while large molecules tend to recognize the major groove binding site [59]. As can be seen, the results of molecular modeling studies confirmed the results of experimental approaches.

The MVD software was also used to characterize the binding mode of FLR at the dsDNA. Fig. 9B shows the groove binding of CD to the major groove of dsDNA. As can be seen FLR is a large molecule which prefers the major groove binding site.

Table 2
Results of applying EQUISPEC.

Analyzed matrix	K_b
$\left[D^{CD}_{SWV} D^{CD}_{LSV} D^{CD}_{F} D^{CD}_{UV-vis}\right]$	4.12×10^4
$\left[D^{dsDNA}_{SWV} D^{dsDNA}_{LSV} D^{dsDNA}_{F} D^{dsDNA}_{UV-vis}\right]$	4.21×10^5
$\begin{bmatrix} D^{CD}_{SWV} D^{CD}_{LSV} D^{CD}_{F} D^{CD}_{UV-vis} \\ D^{dsDNA}_{SWV} D^{dsDNA}_{LSV} D^{dsDNA}_{F} D^{dsDNA}_{UV-vis} \end{bmatrix}$	3.88×10^4

3.14. Analytical applications

Because of having a reversible oxidation for CD at FLR/GCE, SWV technique was chosen for quantitative purposes to obtain more sensitivity. Under the optimized conditions for SWV (step potential 0.002 V, amplitude 0.02 V, frequency 25 Hz, and scan rate 50.0 mV s^{-1}), the FLR/GCE in the presence of 50.0 nM CD (Fig. 10, curve a) detects dsDNA in a concentration range of 0.1–25.0 nM (Fig. 10, curves b–n) with a limit of detection (LOD, $3S_b/b$, S_b is the standard deviation (n = 8) of the blanks, and b is the slope value of the respective calibration graph) of 0.03 nM (the signal at 0.543 V has been used for quantitative purpose, see Fig. 10). Moreover, the sensitivity for dsDNA detection calculated from the slope of the respective calibration graph was to be 0.0235 μA nM^{-1},

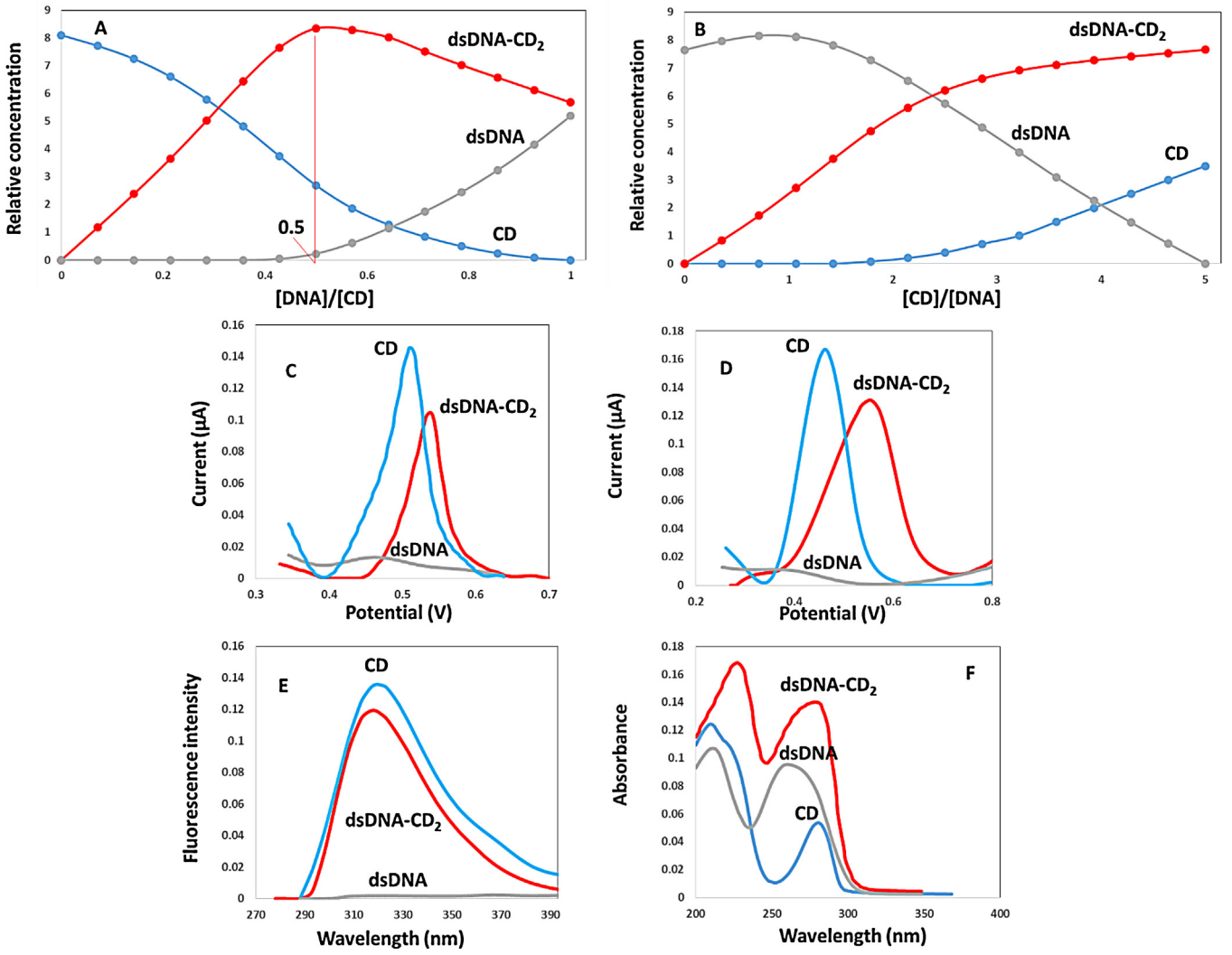

Fig. 8. Results of applying MCR-ALS: (A and B) extracted concentration profiles; (C–F) extracted signal profiles of different species involved in SWV, LSV, F and UV–vis experiments, respectively, obtained from the eight experiments described in Section 2.1.5.

indicating the high sensitivity of the proposed sensing system.

The repeatability and reproducibility of the proposed biosensor were evaluated using SWV. The repeatability of one electrode in the presence of 25.0 nM CD to determine 10.0 nM dsDNA was fairly good. The relative standard deviation (RSD) was 3.58% for 7.0 successive assays. The electrode-to-electrode reproducibility was estimated from the response to 10.0 nM dsDNA in the presence of 25.0 nM CD with 8.0 different sensors and this series yielded a RSD of 4.75%. Stability of the FLR/GCE was investigated by storing at room temperature in presence and absence of PBS (0.05 M, pH 4.0). It was stable for one month and after four weeks a gradual decrease (8.5%) has been found from the current initial values. These results suggested that the FLR/GCE possesses good repeatability and reproducibility and long term stability. Moreover, the FLR/GCE can be prepared within 7.5 min and by manual polishing with alumina slurry we can retain the original nature of the GCE very easily.

To evaluate the selectivity of the proposed sensor, under the optimized conditions, the possible interferences such as L-lysine, L-arginine, L-histidine, L-glutamic acid, ascorbic acid, glucose, uric acid, dopamine, and urea were investigated by premixing with dsDNA (10.0 nM) in the presence of 25.0 nM CD. After the experiment, we concluded that 50.0-fold L-lysine, L-arginine, L-histidine, and L-glutamic acid, 150.0-fold ascorbic acid, glucose, uric acid, dopamine, and urea did not show any remarkable interference effect toward dsDNA determination.

To evaluate the applicability of the present method on real matrices, assays were performed on human serum samples. Recovery experiments were carried out by adding standard solutions of dsDNA to serum matrices. Table 3 summarizes the results obtained for dsDNA determination in human serum samples. The good recoveries suggested that determination of dsDNA using the proposed biosensor was effective and sensitive.

Table 3
Results of analysis of human serum samples ($n = 3$).

Serum sample	Added (nM)	Found (nM)	Recovery (%)
1	2.0	2.1 ± 0.02	104.8
	5.0	5.2 ± 0.04	103.8
	3.0	2.9 ± 0.02	96.7
2	12.0	11.8 ± 0.05	98.3
	8.5	8.7 ± 0.03	102.3
	16.0	16.4 ± 0.05	102.4

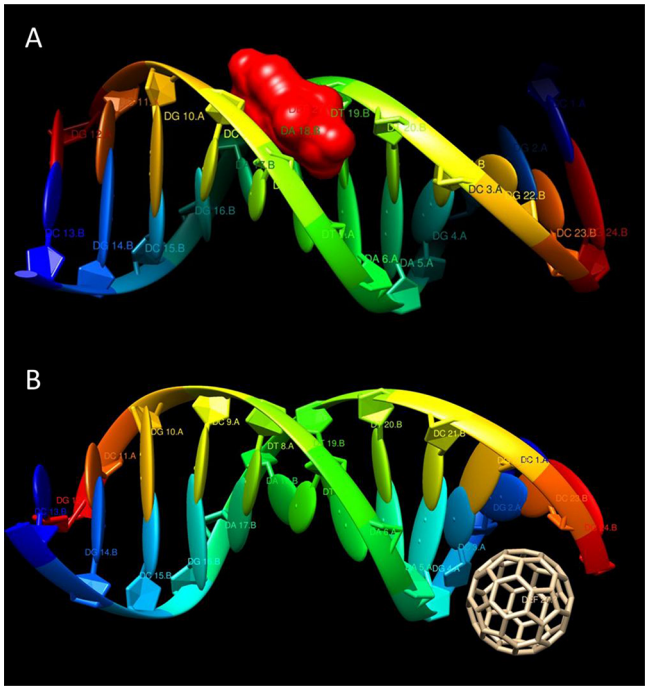

Fig. 9. Results of molecular modeling related to (A) groove binding of CD to the minor groove of dsDNA and (B) groove binding of FLR to the major groove of dsDNA.

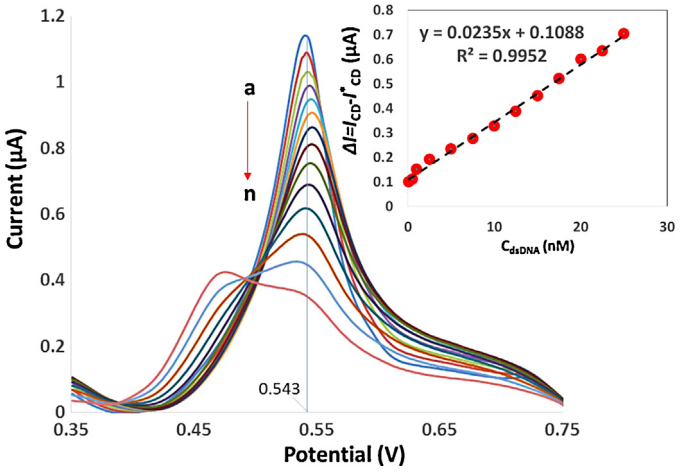

Fig. 10. Square wave voltammograms of 50.0 nM CD (curve a) in PBS (0.05 M, pH 4.0) at FLR/GCE in the presence of increasing concentration of dsDNA (curves b–n: 0.1–25.0 nM), scan rate is 50.0 mV s^{-1}. Inset: Variation of the $\Delta I = I_{CD} - I^*_{CD}$ vs. dsDNA concentration (I_{CD} and I^*_{CD} are SWV signals of CD in the absence and presence of dsDNA, respectively).

4. Conclusion

In this study, the interaction of CD with dsDNA was investigated at a GCE modified with FLR for the first time. The voltammetric studies revealed a remarkable decrease in both anodic and cathodic currents of CD upon the addition of dsDNA with negative, and positive shifts in anodic and cathodic peak potentials, respectively, which indicates the interaction of CD with dsDNA. The FLR/GCE showed an effective electrocatalytic activity toward CD oxidation as well as enhancement of the microscopic area and currents in voltammetric investigations. The binding of CD to dsDNA results in a series of changes in electrochemical behavior and spectral characteristics, confirming that the interaction between CD and dsDNA is groove binding mode. The independent molecular modeling studies resulted in binding mechanism very close to the experimental one. The application of the MCR-ALS for the resolution of the expanded data matrix produced the estimates of the pure signals of CD, and dsDNA which were in good agreement with the measured responses. Additionally and importantly, the voltammetric and spectroscopic signals of the interaction product, dsDNA–CD_2, was extracted. Equilibrium concentration profiles were also obtained. The results showed that the MCR-ALS is a powerful chemometric tool to resolve complex combined data and showed significant potential for investigating the mechanism of the interaction of dsDNA with targeting small compounds at the molecular level. Finally, SWV technique was applied for determination of dsDNA in human serum samples due to observing a reversible oxidation behavior for CD at the FLR/GCE which could obtain more sensitivity by SWV. The combination of voltammetric and spectroscopic methods is of potential importance in understanding the mechanism of binding of small molecules to biological macromolecules.

Acknowledgments

The authors gratefully acknowledge the financial support of this study by Razi University Research Council, UNL, CONICET and ANPCyT.

Appendix A. Supplementary data

Supplementary data associated with this article can be found, in the online version, at http://dx.doi.org/10.1016/j.ijbiomac.2014.05.074.

References

[1] J.A. Gilbert, L.M. Frederick, M.M. Ames, Clin. Cancer Res. 6 (2000) 4365–4372.
[2] H. Li, W. Mei, Z. Xu, D. Pang, L. Ji, Z. Lin, J. Electroanal. Chem. 600 (2007) 243–250.
[3] M.L. Yola, N. Ozaltın, J. Electroanal. Chem. 653 (2011) 56–60.
[4] R. Meunier-Prest, A. Bouyon, E. Rampazzi, S. Raveau, P. Andreoletti, M. Cherkaoui-Malki, Biosens. Bioelectron. 25 (2010) 2598–2602.
[5] A.M.O. Brett, T.R.A. Macedo, D. Raimundo, M.H. Marques, S.H.P. Serrano, Biosens. Bioelectron. 13 (1998) 861–867.
[6] Y.S. Kim, H.S. Jung, T. Matsuura, H.Y. Lee, T. Kawai, M.B. Gu, Biosens. Bioelectron. 22 (2007) 2525–2531.
[7] H.W. Kroto, J.R. Heath, S.C. O'Brien, R.F. Curl, R.E. Smalley, Nature 318 (1985) 162–163.
[8] S. Griese, D.K. Kampouris, R.O. Kadara, C.E. Banks, Electroanalysis 20 (2008) 1507–1512.
[9] E. Nakamura, H. Isobe, Acc. Chem. Res. 36 (2003) 807–815.
[10] C.A. Martin, D. Ding, J.K. Sørensen, T. Bjørnholm, J.M. van Ruitenbeek, H.S.J. van der Zant, J. Am. Chem. Soc. 130 (2008) 13198–13199.
[11] J.T. Robinson, F.K. Perkins, E.S. Snow, Z. Wei, P.E. Sheehan, Nano Lett. 8 (2008) 3137–3140.
[12] B.C. Thompson, J.M.J. Frechet, Angew. Chem. Int. Ed. 47 (2008) 58–77.
[13] D.O. Wood, J.S. Lee, J. Inorg. Biochem. 2 (2005) 566–574.
[14] F. Westerlund, P. Lincoln, Biophys. Chem. 1 (2007) 11–17.
[15] N. Kanayama, T. Takarada, H. Shibata, A. Kimura, M. Maeda, Anal. Chim. Acta 619 (2008) 101–109.
[16] B. Pagano, A. Virno, C.A. Mattia, L. Mayol, A. Randazzo, C. Giancola, Biochimie 90 (2008) 1224–1232.
[17] F. Sousa, D.M.F. Prazeres, J.A. Queiroz, Arch. Biochem. Biophys. 2 (2007) 154–162.
[18] Y.N. Ni, D.Q. Lin, S. Kokot, Talanta 5 (2005) 1295–1302.
[19] Z.S. Wu, J.H. Jiang, L. Fu, G.L. Shen, R.Q. Yu, Anal. Biochem. 353 (2006) 22–29.
[20] X. Tian, F.J. Li, L. Zhu, B.X. Ye, J. Electroanal. Chem. 621 (2008) 1–6.
[21] M.T. Carter, M. Rodriguez, A.J. Bard, J. Am. Chem. Soc. 11 (1989) 8901–8911.
[22] E. Palecek, Electroanalysis 21 (2009) 239–251.
[23] J. Jaumot, A. Avino, R. Eritja, R. Tauler, R. Gargallo, J. Biomol. Struct. Dyn. 21 (2003) 267–278.
[24] A. de Juan, A. Izquierdo-Ridorsa, R. Tauler, G. Fonrodona, E. Casassas, Biophys. J. 73 (1997) 2937–2948.
[25] Y.N. Ni, Q.L. Zhang, S. Kokot, Analyst 135 (2010) 2059–2068.
[26] R. Gargallo, M. Vives, R. Tauler, R. Eritja, Biophys. J. 81 (2001) 2886–2896.
[27] S. Navea, A. de Juan, R. Tauler, Anal. Chem. 74 (2002) 6031–6039.

[28] M.E. Reichman, S.A. Rice, C.A. Thomas, P.A. Doty, J. Am. Chem. Soc. 76 (1954) 3047–3053.
[29] http://www.rcsb.org./pdb
[30] http://www.ub.es/gesq/mcr/mcr.htm
[31] M. Esteban, C. Arïo, J.M. Díaz-Cruz, M.S. Diaz-Cruz, R. Tauler, Trends Anal. Chem. 19 (2000) 49–61.
[32] M. Esteban, C. Arïno, J.M. Díaz-Cruz, Trends Anal. Chem. 25 (2006) 86–92.
[33] H. Gampp, M. Maeder, C.J. Meyer, A.D. Zuberbühler, Talanta 32 (1985) 1133–1139.
[34] H. Abdollahi, V. Mahdavi, Langmuir 23 (2007) 2362–2368.
[35] S. Perez, M.J. Culzoni, G.G. Siano, M.D. Gil Garcia, H.C. Goicoechea, M.M. Galera, Anal. Chem. 81 (2009) 8335–8346.
[36] M. Vives, R. Gargallo, R. Tauler, Anal. Chem. 71 (1999) 4328–4337.
[37] C.B. Zachariassen, J. Larsen, F. Van den Berg, R. Bro, A. De Juan, R. Tauler, Chemom. Intell. Lab. Syst. 83 (2006) 13–25.
[38] R. Tauler, A. Izquierdo-Ridorsa, E. Casassas, Chemom. Intell. Lab. Syst. 18 (1993) 293–300.
[39] R. Tauler, A.K. Smilde, B.R. Kowalski, J. Chemom. 9 (1995) 31–58.
[40] A. Radi, M.A. El Ries, S. Kandil, Anal. Chim. Acta 495 (2003) 61–67.
[41] S.S. Kalanur, J. Seetharamappa, S.N. Prashanth, Colloids Surf. B 82 (2011) 438–442.
[42] S.F. Wang, T.Z. Peng, C.F. Yang, Electroanalysis 14 (2002) 1648–1653.
[43] F. Qu, N.Q. Li, Y.Y. Jiang, Talanta 45 (1998) 787–793.
[44] F. Wang, Y. Xu, J. Zhao, S. Hu, Bioelectrochemistry 70 (2007) 356–362.
[45] X. Tian, Y. Song, H. Dong, B. Ye, Bioelectrochemistry 73 (2008) 18–22.
[46] A.J. Bard, L.R. Faulkner, Electrochemical Methods Fundamentals and Applications, 2nd ed., John Wiley and sons, New York, 2001.
[47] L.S. Lerman, J. Mol. Biol. 3 (1961) 18–30.
[48] G. Zhang, P. Fu, J. Pan, J. Lumin. 134 (2013) 303–307.
[49] Y. Fei, G. Lu, G. Fan, Y. Wu, Anal. Sci. 25 (2009) 1335–1341.
[50] J.R. Lakowicz, Principles of Fluorescence Spectroscopy, 2nd ed., Plenum Press, New York, 1999, pp. 237.
[51] X.Z. Feng, Zh. Lin, L.J. Yang, Ch. Wang, Ch.l. Bai, Talanta 47 (1998) 1223–1229.
[52] Y. Ni, D. Lin, S. Kokot, Talanta 65 (2005) 1295–1302.
[53] Y. Cao, X.W. He, Spectrochim. Acta A 54 (1998) 883–892.
[54] X. Ling, W. Zhong, Q. Huang, K. Ni, J. Photochem. Photobiol. B 93 (2008) 172–176.
[55] R. Marty, N.Ch. Nsoukpoe-Kossi, D. Charbonneau, C.M. Weinert, L. Kreplak, H.A. Tajmir-Riahi, Nucleic Acids Res. 37 (2009) 849–857.
[56] A. De Juan, S. Navea, J. Diework, R. Tauler, Chemom. Intell. Lab. Syst. 70 (2004) 11–21.
[57] A. Dominguez-Vidal, M.P. Saena-Navajas, M.J. Ayora-Canada, B. Lendl, Anal. Chem. 78 (2006) 3257–3264.
[58] R.M. Dyson, S. Kaderli, G.A. Lawrance, M. Maeder, A.D. Zuberbühler, Anal. Chim. Acta 353 (1997) 381–393.
[59] R. Hajian, M. Tavakol, J. Chem. 9 (2012) 471–480.